Available online at www.sciencedirect.com
ScienceDirect
Journal of Power Sources 161 (2006) 666–675
JOURNAL OF POWER SOURCES
www.elsevier.com/locate/jpowsour

Corrosion management of PbCaSn alloys in lead-acid batteries: Effect of composition, metallographic state and voltage conditions

E. Rocca *, G. Bourguignon, J. Steinmetz

Université Henri Poincaré-Nancy I, Laboratoire de Chimie du Solide Minéral UMRCNRS 7555, BP239, 54506 Vandoeuvre-Les-Nancy, France

Received 15 November 2005; received in revised form 22 March 2006; accepted 10 April 2006
Available online 7 July 2006

Abstract

Since several years, lead calcium-based alloys have supplanted lead antimony alloys as structural materials for positive grids of lead-acid batteries in many applications, especially for VRLA batteries. Nevertheless, the positive grid corrosion probably remains one of the causes of rapid and premature failure of lead-acid batteries. The objective of the present study is to present a comprehensive study of the PbCaSn alloy corrosion in function of their composition, metallographic state and voltage conditions (discharge, overcharge, floating and cycling conditions). For that, four alloys PbCaSn x wt.% ($x = 0$, 0.6, 1.2, 2) were synthesized in two extreme metallurgical conditions and tested by four electrochemical lab-tests. Weight loss measurements and analyses by SEM, EPMA and XRD allowed to monitor the oxidation tests and to characterize the corrosion layers after the oxidation tests.

The results show that the tin level in PbCaSn alloys should be adapted on the calcium concentration and the rate of overageing process, to maintain the beneficial effect of tin in service during the battery lifetime. According to our results, a Sn/Ca ratio of 2.5 gives good corrosion resistance in all potential conditions. Nevertheless, when tin level is too high, the corrosion layers can peel off from the metal, which involves a lack of cohesion between the collector and the paste, in cycling conditions.

The anodic potential undergone by the metal is a second main factor determining the corrosion, especially the floating conditions and the frequency of deep discharge and overcharge. Thus the adjustment of the charge controller parameters of a battery system is a necessity to increase the lifetime of the grids and maintain a good rechargeability.

Keywords: Corrosion; Lead-acid batteries; Lead alloys

1. Introduction

Since 10 years, several ageing processes of lead-acid batteries leading to a loss of capacity were identified and reviewed [1–4]. Three main kinds of premature capacity loss are now accepted. The first one, named PCL-1, results in an increase of the resistance between the positive active mass and the metallic grid, and is general due to the growth of an insulate corrosion layer on the grid. The second capacity loss, named PCL-2, is the result of a swelling and a loss of cohesion of positive active mass, due to the growth of coarse $PbSO_4$ crystals during the charge/discharge cycles. More recently, a third mechanism of capacity loss especially in VRLA batteries was mentioned. It is the consequence of the oxygen cycle and is named PCL-3. In fact, the electrochemical reduction of a large quantity of oxygen on the negative plates depolarizes the negative electrode, and may lead to a possible degradation by an irreversible sulfatation process.

The current collector in lead alloys is the strong advantage but also the weak point of lead-acid batteries. Indeed lead alloys assure a good chemical continuity between the lead oxide active mass and the collector responsible for the good adherence of the active mass. Nevertheless lead alloys are subjected to corrosion phenomenon in sulfuric acid.

During the past 10 years, the development of lead calcium-based alloys have produced an important improvement of lead-acid batteries leading to use new grid manufacturing processes such as continuous casting, rolling, expanding of the alloys, and manufacturing of low-maintenance batteries such as VRLA batteries [5,6].

* Corresponding author. Tel.: +33 3 83 68 46 68; fax: +33 3 83 68 46 11.
E-mail address: emmanuel.rocca@lcsm.uhp-nancy.fr (E. Rocca).

0378-7753/$ – see front matter © 2006 Elsevier B.V. All rights reserved.
doi:10.1016/j.jpowsour.2006.04.140

Nowadays, lead calcium-based alloys have replaced lead antimony alloys as structural materials for positive grids of lead-acid batteries in many applications. Nevertheless, the positive grid corrosion probably remains one of the causes of rapid and premature failure of lead-acid battery, especially for the automotive batteries and stand-by applications, as been reported by many studies [2–7].

Two main types of PbCaSn alloy corrosion were generally reported in the literature [8,9]:

- The growth of a PbO layer between the alloy and the active mass in the deep discharge conditions. Because of the poor electric conductivity of PbO, the recharge of the active mass becomes very difficult and almost impossible in some cases.
- The oxidation of lead into PbO_2 at high anodic potential. This kind of corrosion provokes the irreversible consummation of metal by forming large pits then can induce the mechanical break of the grids. This phenomenon occurs in overcharge conditions especially during the charge at high current called sometimes "boost charge".

So, the parameters of the charge controller which regulates the floating conditions, the depth of discharge and the charge (and "boost charge") of batteries in service seems to be one of the main factors influencing the lifetime of the grid. The composition of lead–calcium–tin alloys is also the subject of many questions and studies in the literature. The incorporation of tin is now accepted as a solution to reduce the corrosion problems in positive grids. However, according to the Prengaman's observations, a very corrosion-resistant alloy for the positive grid may be a disadvantage for the battery service [10].

So, for a same set of alloys, the purpose of this work was to obtain an understanding description of the corrosion behavior of PbCaSn alloys at several anodic potential simulating different batteries conditions: the deep discharge, the overcharge, the floating conditions and a typical charge–discharge cycle of a lead-acid battery. This corrosion behavior was studied in function of tin content and metallurgical state of alloys. In fact, the hardness of PbCaSn alloys increases with time after casting, leading first to the aged metallurgical state, through the continuous precipitation in the lead matrix of very fine intermetallic phase, $(Pb_{1-x}Sn_x)_3Ca$. With time, these metallurgical transformations of ageing are followed by a discontinuous precipitation, which provokes a large decrease of the alloy hardness. This last metallurgical state called overageing results on a lamellar and coarse precipitation of the $(Pb_{1-x}Sn_x)_3Ca$ phases [11].

For this study, PbCaSn x wt.% ($x = 0$, 0.6, 1.2, 2) alloys were cast in the same conditions and stabilized with different thermal treatments in a given metallurgical state. Electrochemical measurements allowed monitoring the oxidation tests. Then optical microscopy (OM), scanning electron microscopy (SEM), electron probe microanalysis (EPMA) and X-ray diffraction (XRD) were used to characterize the corrosion layers.

2. Experimental

2.1. Synthesis of alloys

The Pb–Ca 0.08 wt.%–Sn x wt.% alloys (with $x = 0$, 0.6, 1.2, 2) were synthesised from Pb–Ca 0.12 wt.% master alloy produced by CEAC (Compagnie Européenne des Accumulateurs), pure lead (99.95% GoodFellow) and pure tin (99.99% Prolabo). The raw materials were melted in alumina crucibles for 1 h at 650 °C under nitrogen flux, and casting in an iced copper mould to form plates with a size of 60 mm × 60 mm × 3 mm. After casting, the composition of each alloy was verified by atomic absorption spectroscopy once it was chemically dissolved.

After casting, the alloys were treated by different thermal treatments according to the Transformation–Time–Temperature curve (TTT) of the alloys [12]. A typical TTT curve of PbCaSn alloy is displayed in Fig. 1

- The first treatment is only a 6-month ageing at room temperature during 6 months for reaching the B zone of the TTT diagram. These treated alloys are noted aged.
- The second treatment is performed at 120 °C during 3 month to reach the overaged state or the C zone of the TTT diagram (Fig. 1). These samples were called overaged.

The grain size and the metallographic microstructure were checked by optical microscopy after dipping in a CH_3COOH/H_2O_2 solution (80/20 in vol.), and then in a citric acid/molybdate ammonium one (250/100 g l^{-1})

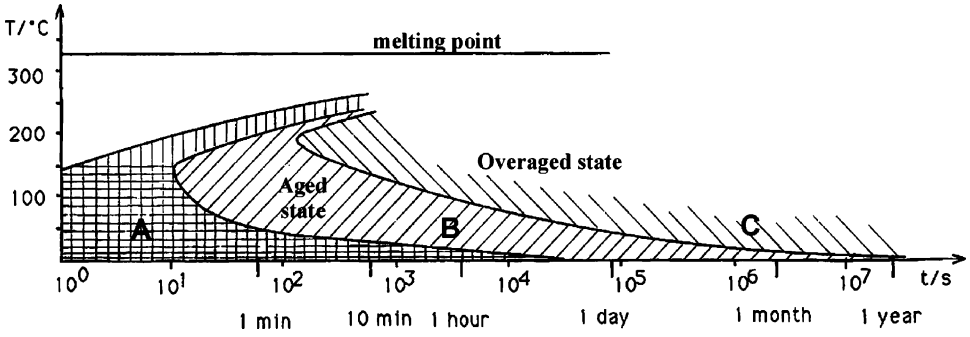

Fig. 1. Typical Temperature–Transformation–Time diagram (TTT diagram) of Pb–Ca 0.11 wt.%–Sn 0.57 wt.%. Zone A: discontinuous transformation; zone B: continuous precipitation of $(Pb_{1-x}Sn_x)_3Ca$; zone C: discontinuous precipitation of lamellar $(Pb_{1-x}Sn_x)_3Ca$.

Table 1
Alloy description (grain size, type of heat treatment and Vickers hardness after heat treatment)

Pb–Ca 0.08 wt.%–Sn *x* wt.% (wt.%)	Grain size (μm)	Heat treatment	Hardness (Hv)
0	100 ± 10	Aged, overaged	13, 7
0.6	120 ± 10	Aged, overaged	16, 8
1.2	140 ± 15	Aged, overaged	17, 8
2	120 ± 15	Aged, overaged	18, 11

2.2. Oxidation tests

Electrochemical tests were performed in a three-electrode electrochemical cell connected to an EG & G Princeton 273 A potentiostat driven by a computer. The lead alloys used as working electrode (2.8 cm^2) was a disk of 3 cm of diameter. It was placed horizontally at the bottom of the cell under a Pt-grid (50 cm^2) used as auxiliary electrode. The distance between working and auxiliary electrode was 2 cm. Only one side of the working electrode was in contact with electrolyte. The amount of the electrolyte was 70 ml. The reference electrode was a K_2SO_4-saturated mercurous sulfate electrode (E = +0.658 V versus SHE), and all working electrode potentials are given versus this reference electrode.

The working electrode was mechanically polished with successively finer grades of SiC emery papers up to 1200, then with colloidal silica dispersed in water (particle size: 0.1 μm). Samples were finally rinsed with distilled water and ethanol then dried.

Four oxidations tests were set up according the battery manufacturers and literature reporting potential measurements of positive grid in batteries in service. These tests are described below:

- *The discharge tests*: The first test was in deep discharge conditions at +0.7 V for 7 days in 0.5 M H_2SO_4 at room temperature. The second one is close to the conditions of usual discharge state, at +0.9 V for 7 days in 0.5 M H_2SO_4.
- *The overcharge test*: +1.5 V for 5 days in 5 M H_2SO_4 at 50 °C.
- *The floating test*: +1.1 V for 7 days in 0.5 M H_2SO_4 at room temperature.
- *The cycling test*: A cycle is composed of 2 h of overcharge at 1.5 V, a potential decrease at 0.2 mV s^{-1} until 0.7 V, 2 h of deep discharge time at 0.7 V, finally a potential increase until

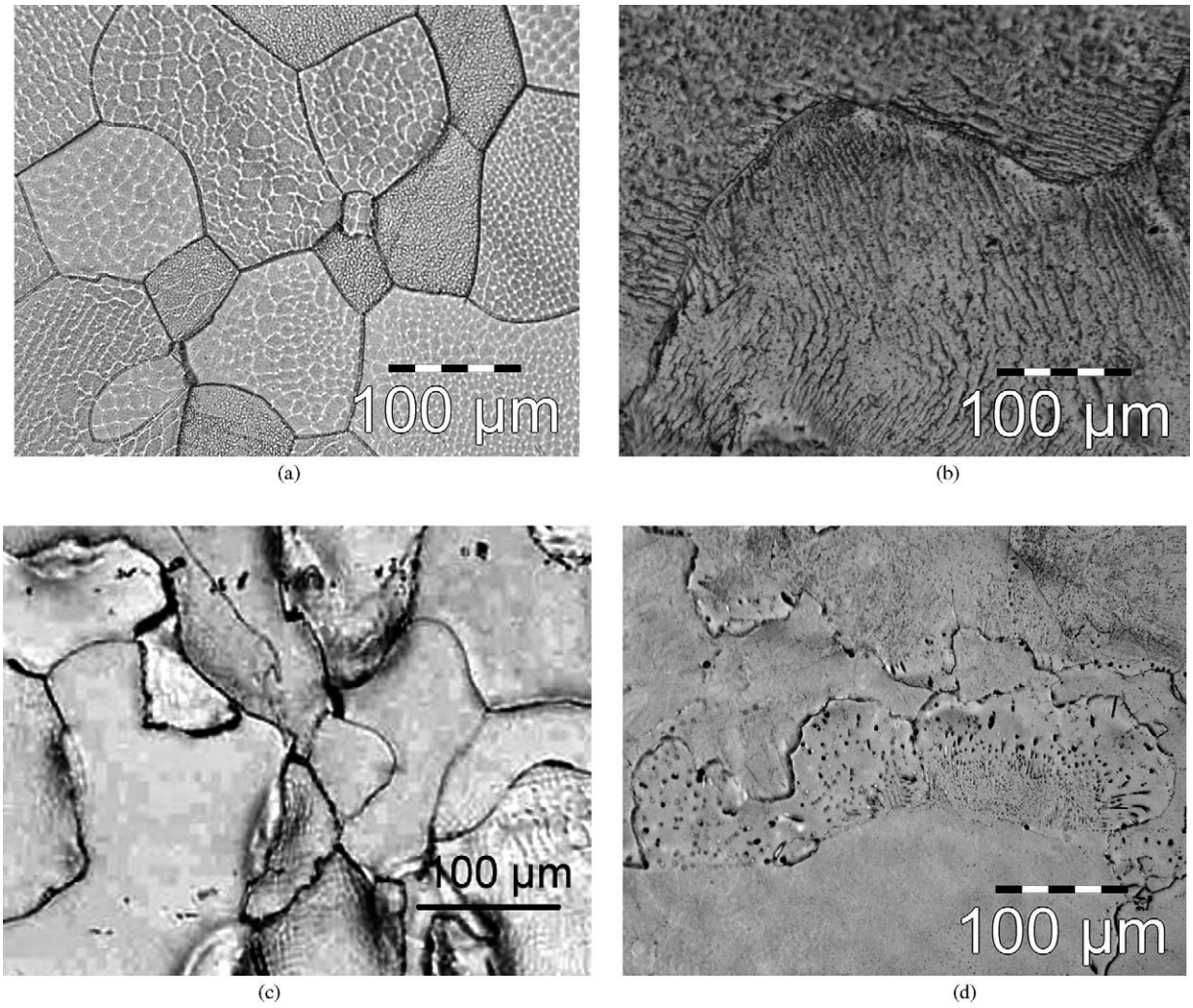

(a) (b) (c) (d)

Fig. 2. OM micrograph of PbCaSn 0.6 wt.% (a and b) and PbCaSn 2 wt.% (c and d) in metallurgical aged state (a and c) and overaged state (b and d).

1.5 V. This test goes on for 20 cycles, or 5 days in 5 M H_2SO_4 at room temperature.

In these conditions of tests, no stratification and density change of H_2SO_4 electrolyte was observed. In addition, in overcharge conditions (high voltage), the volume of gas produced by the working and auxiliary electrodes was measured. The oxygen volume was deduced by calculation of the hydrogen volume by assuming that the total current measured between the two electrodes was used for the reduction of water in hydrogen gas on the Pt-grid auxiliary electrode.

2.3. Corrosion layer analysis

After the oxidation tests, the samples were embedded in epoxy resin and the metallographic cross-sections were polished in the same way as the working electrode.

The XRD and SEM techniques (Hitachi S-2500 equipped with a EDS detector) was applied to determine the morphology and the composition of the corrosion layers. EPMA (Cameca SX-50 apparatus) analysis was used to precise the compositions in some cases. For the overcharge test, the corrosion of the alloys was characterized through metallic weight loss measurements. The sample weight was measured before oxidation and after dissolution of the corrosion products after test in acetic acid, hydrazine, water solution (1/3, 1/3, 1/3 in vol.).

3. Results

3.1. Characterization of alloys

The cross-section of each alloy was observed after metallographic chemical attack. The grain sizes, listed in Table 1, are almost similar for the entire alloy, around 120 μm (Fig. 2). Fig. 2(a) and (b) show typical micrographs of aged state and complete overaged state for the PbCaSn 0.6 wt.% alloy. On Fig. 2(b) (overaged state), the dissolution of the coarse precipitates during the metallographic etching induces an important roughness, and partially masks the grain boundaries. These two different metallurgical states are also characterized by different

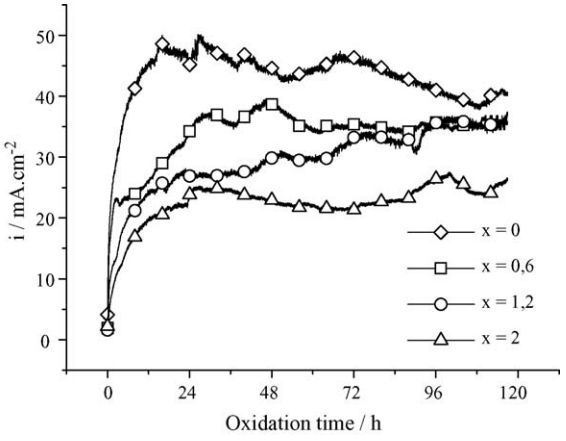

Fig. 3. $i = f(t)$ curves during the oxidation of aged PbCaSn alloys in overcharged conditions (+1.5 V, 5 M H_2SO_4, 50 °C).

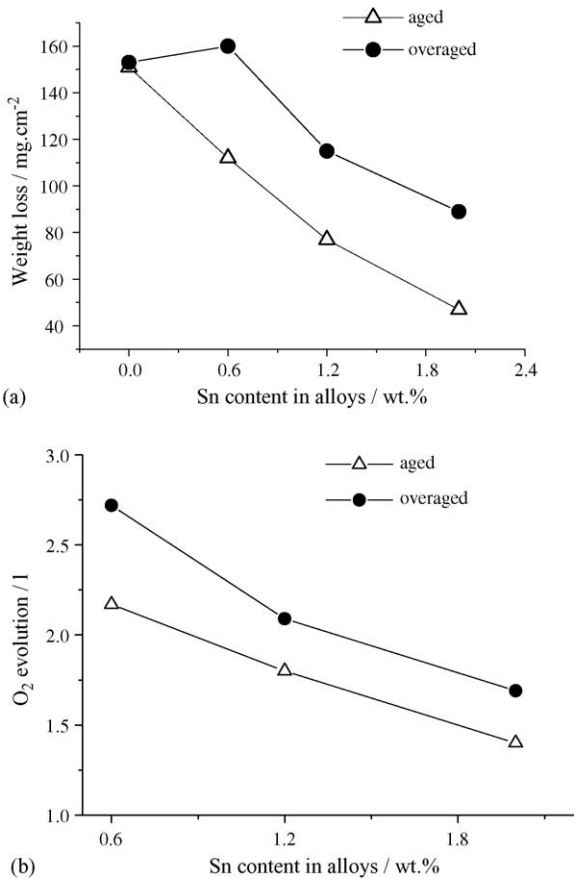

Fig. 4. (a) Weight loss and (b) oxygen gas evolution of PbCaSn alloys after 5 days of oxidation in overcharged conditions (+1.5 V, 5 M H_2SO_4, 50 °C).

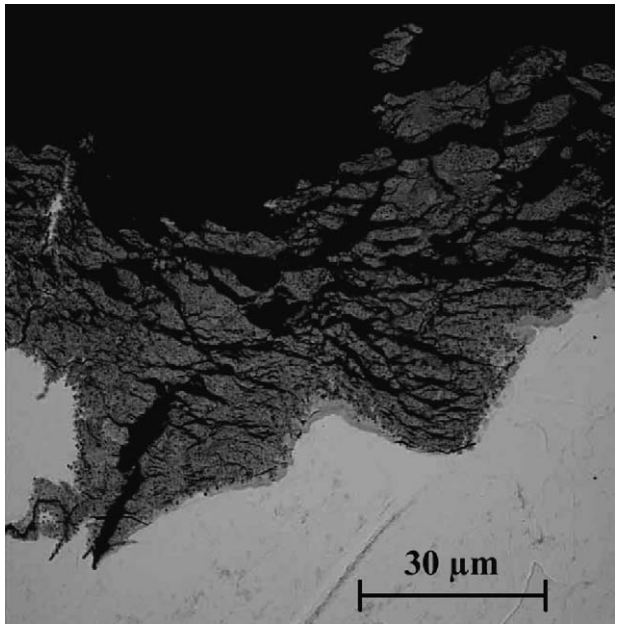

Fig. 5. Typical metallographic cross section of PbCaSn alloys after 5 days of oxidation in overcharged conditions (+1.5 V, 5 M H_2SO_4, 50 °C).

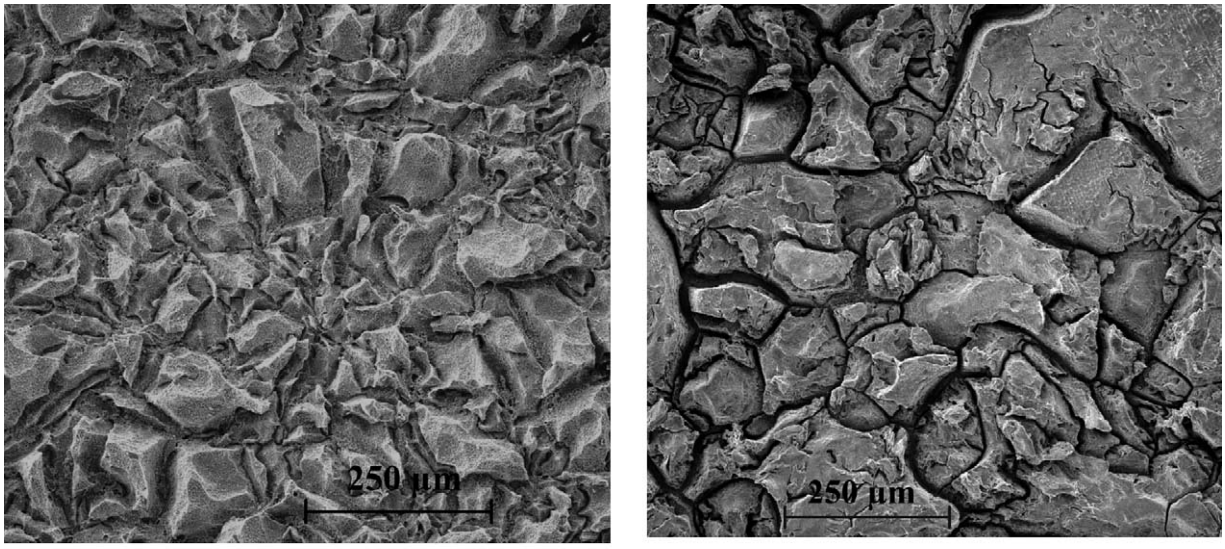

Fig. 6. SEM observations of pickled surface: PbCaSn 0 wt.% (a) and PbCaSn 2 wt.% (b) after the overcharged test of metallic surfaces.

hardness values as mentioned in Table 1. The aged alloys have the highest Vickers value due to the precipitation of a nanometric $(Pb_{1-x}Sn)_3Ca$ intermetallic phase in the α-lead matrix through a continuous transformation. In opposite, the hardness of the overaged alloys is close to that of pure lead because of the coalescence of the fine precipitates to form coarse and less hardening $(Pb_{1-x}Sn)_3Ca$ precipitates through a discontinuous precipitation. On the micrograph of the PbCaSn 2 wt.% overaged alloy, we can observe that the grains are only partially overaged even after several months of treatment at 120 °C (Fig. 2(d)). This observation explains that the hardness value of overaged PbCaSn 2 wt.% remains high. As observed by several authors in the literature, the presence of high content of tin inhibits the overageing process of PbCa alloys [12,13].

3.2. Overcharge tests

At +1.5 V in 5 M H_2SO_4, the current recorded during the overcharge test for the set of the aged alloys is almost constant with time, as observed in Fig. 3. The measurements for the overaged alloys show the same behavior. In all cases, presence of tin leads to a decrease of the oxidation current, which is correlated to a decrease of the weight loss of alloys due to corrosion and a decrease of the oxygen evolution, as displayed in Fig. 4(a) and (b). According to measurements of the oxygen gas evolution, weight loss and current, the calculation of the faradic rate of each process (oxygen release and corrosion) shows that 99.5–99.9% of the oxidation current is due to the water oxidation to oxygen. According to Fig. 4, the presence of tin increases the oxygen evolution overvoltage of the alloys.

After the overcharge test, SEM analyses of the cross sections of all alloys present a thick corrosion layer mainly constituted by β-PbO_2 and a deep intergranular corrosion (Fig. 5). As shown in Fig. 6, after removing of the corrosion products, both intergranular and intragranular corrosions are important; nevertheless, the intragranular corrosion is markedly reduced in presence of tin, which explains the lower weight loss of PbCaSn 2 wt.% in comparison to PbCaSn 0 and 0.6 wt.%.

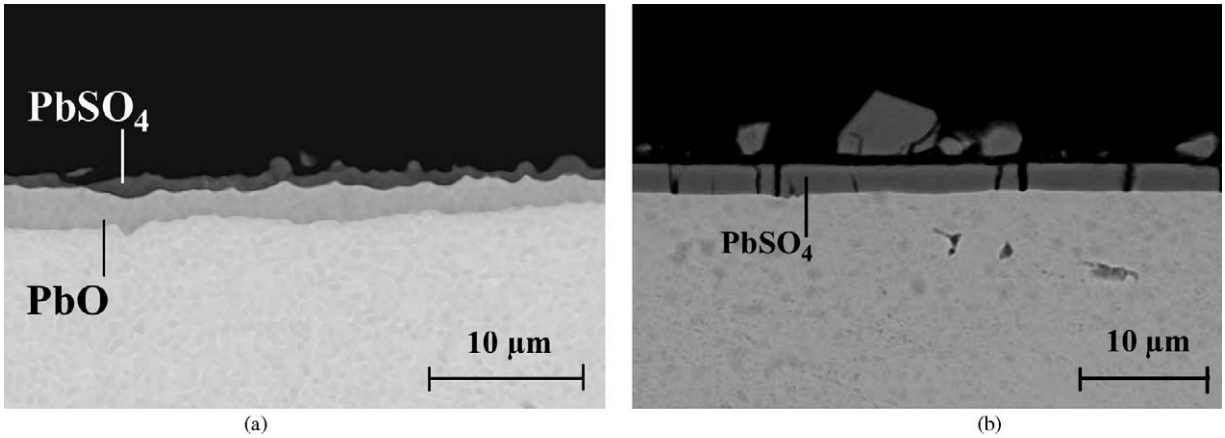

Fig. 7. Typical SEM micrographs on PbCaSn 0.6 wt.% (a) and PbCaSn 2 wt.% after oxidation during 7 days in deep discharge conditions (+0.7 V, H_2SO_4 0.5 M, room temperature).

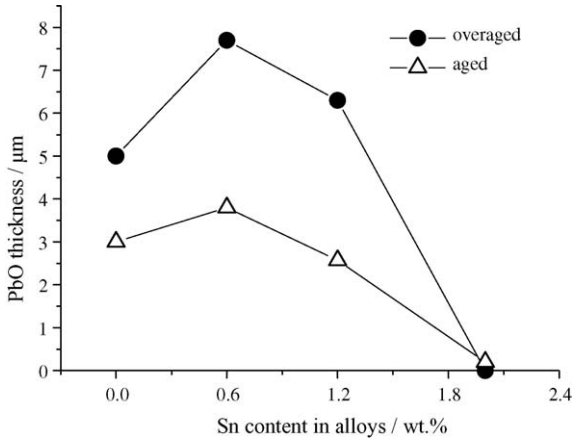

Fig. 8. Thickness of PbO layer measured on PbCaSn alloys after oxidation for 7 days in deep discharge conditions (+0.7 V, H_2SO_4 0.5 M, room temperature).

3.3. Discharge and deep discharge tests

In conditions of deep discharge at +0.7 V, all the PbCaSn alloys are covered with a duplex corrosion layer constituted with α-PbO and lead sulfate $PbSO_4$, except the most tin-concentrated alloy, PbCaSn 2 wt.%, for which only $PbSO_4$ is detected as corrosion product (Fig. 7(a) and (b)).

After 7 days of oxidation, the curves of PbO thickness versus tin content in PbCaSn alloys exhibit a usual bell-shape reported also by a previous study for 1 day of oxidation (Fig. 8) [14]. This behavior is similar for the two series of alloys with a higher maximum for the overaged one. No PbO is present on the PbCaSn 2 wt.%, whatever the metallurgical state after 7 days of deep discharge test.

The aged alloys were also oxidized at a higher potential, +0.9 V, which is representative of the normal discharge of the lead-acid batteries. After 7 days of oxidation, the SEM and EPMA analysis of the low tin-concentrated alloys cross-sections reveal a complex corrosion layer, $PbO/PbO_x/PbSO_4$, with a thick

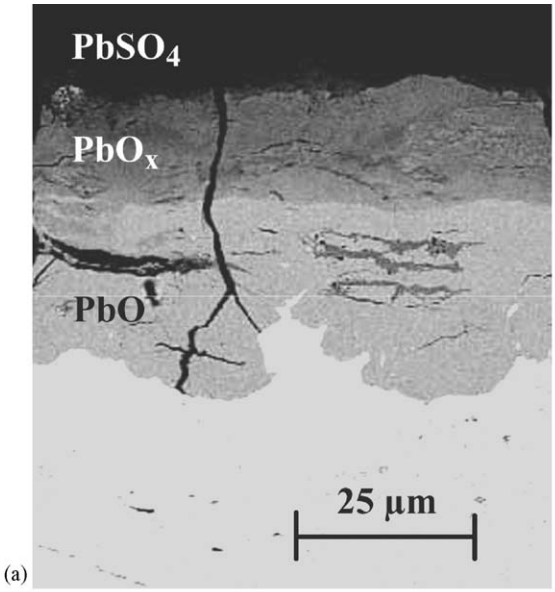

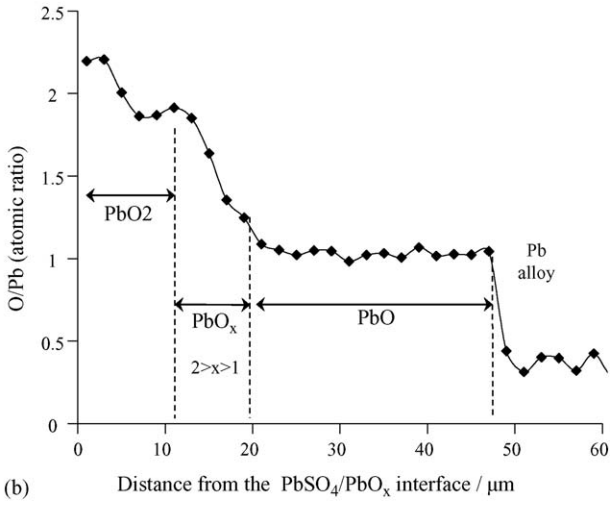

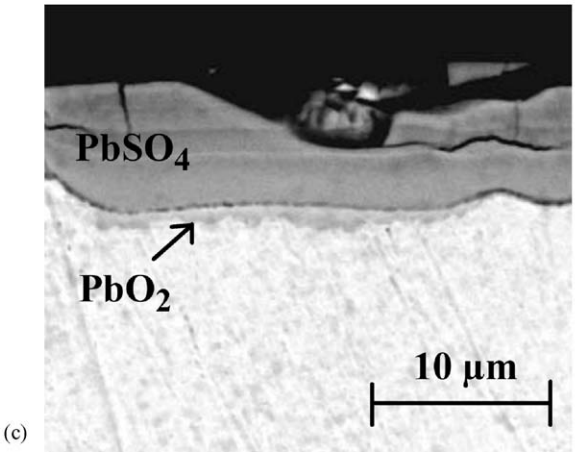

Fig. 9. Metallographic cross-sections of aged PbCaSn alloys after oxidation during 7 days in modified deep discharge conditions (+0.9 V, H_2SO_4 0.5 M, room temperature). (a) PbCaSn 0.6 wt.%; (b) EPMA analysis of the corrosion layer of PbCaSn 0.6 wt.%; (c) PbCaSn 2 wt.%.

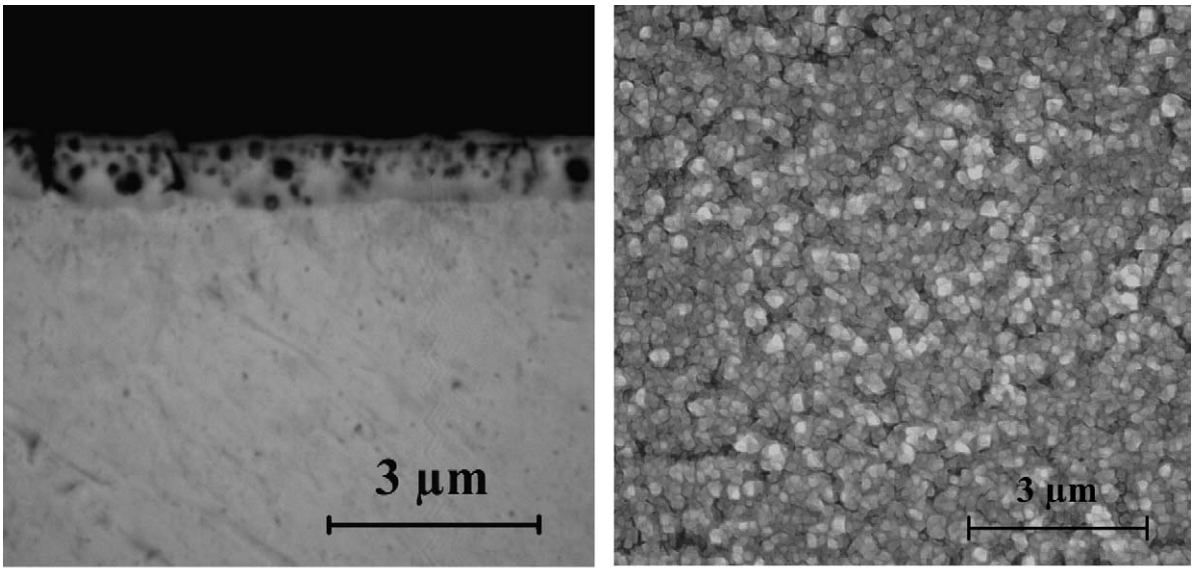

Fig. 10. Typical observations of PbCaSn alloys after oxidation in floating conditions (+1.1 V, 5 M H_2SO_4, room temperature): (a) metallographic cross-section and (b) surface.

layer of α-PbO, as observed in Fig. 9(a) and (b). In contrast, the oxidation of a PbCaSn 2 wt.% leads to a thinner layer, having only a duplex PbO_2/$PbSO_4$ structure (Fig. 9(c)).

3.4. Floating conditions

After an oxidation at +1.1 V in 5 M H_2SO_4 at room temperature for 5 days, all the PbCaSn tested alloys display the same kind of corrosion layer. A typical example is displayed in Fig. 10. The measured oxidation current is particularly very low, and the corrosion layer is very thin, below 1–2 μm. It is mainly constituted by β-PbO_2 containing a small part of α-PbO_2 according to XRD analysis. These observations are consistent with the work of some authors claiming that the corrosion rate of lead in sulfuric acid presents a minimum for oxidation potentials in a range of +1 to +1.3 V [15,4].

3.5. Cycling conditions

Only the aged alloys were tested in cycling conditions. The potential cycle and a typical current transient are displayed in Fig. 11. In these conditions of tests, no significant change of charge during the successive cycles was observed in function of time. The current peaks observed during the increase and decrease of potential corresponds to the classical oxidation and reduction peaks recorded on a lead alloys voltamperogram [16,14]. Fig. 12 shows the metallographic cross-sections observed after the cycling test in function of the tin content in the alloys. The overall corrosion layer thickness decreases with the increase of the tin content in alloys. The cross sections, displayed in Fig. 12(a) and (b) for PbCaSn 0 and 0.6 wt.%, present a corrosion layer with a lamellar structure formed by successive layers of PbO and PbO_2. For the low tin content alloys, the corrosion layers are thick (around 20–30 μm), compact and adhesive to the metal. The tests are stopped after the deep discharge step which explains presence of a thick PbO layer at the interface metal/corrosion layer. In contrast, on the high tin content alloys (1.2 and 2 wt.%), the corrosion layers are thinner, contain no visible PbO layer, and seem to be more homogenous; but they are more brittle than that growing on low tin content alloys and easily peeled off from the metal (Fig. 12(c) and (d)).

4. Discussion

For increasing the specific energy of the lead-acid batteries, the reduction of the inactive material in the plate can be reached by the choice of a corrosion-resistant alloy to manufacture the current collector and the mechanical holder for the active mass. However, the control of the corrosion phenomenon is essential to design the grid and to increase its lifetime.

Through the results of this study, the management of the corrosion phenomenon of PbCaSn alloys depends on three main factors: the metallurgical state of the alloys, their composition especially the tin level and the electrochemical potential of the metal.

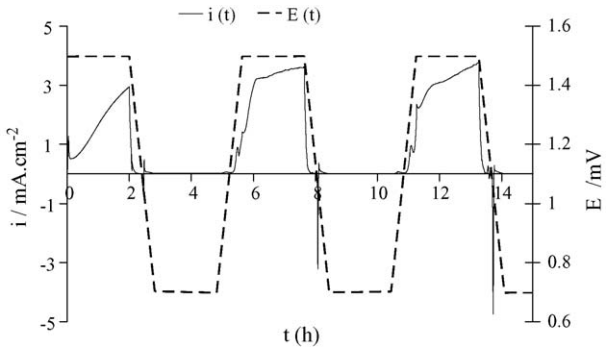

Fig. 11. Potential cycle $E = f(t)$ of the cycling test (a) and typical current transient curve $i = f(t)$ recorded during the cycling test (b).

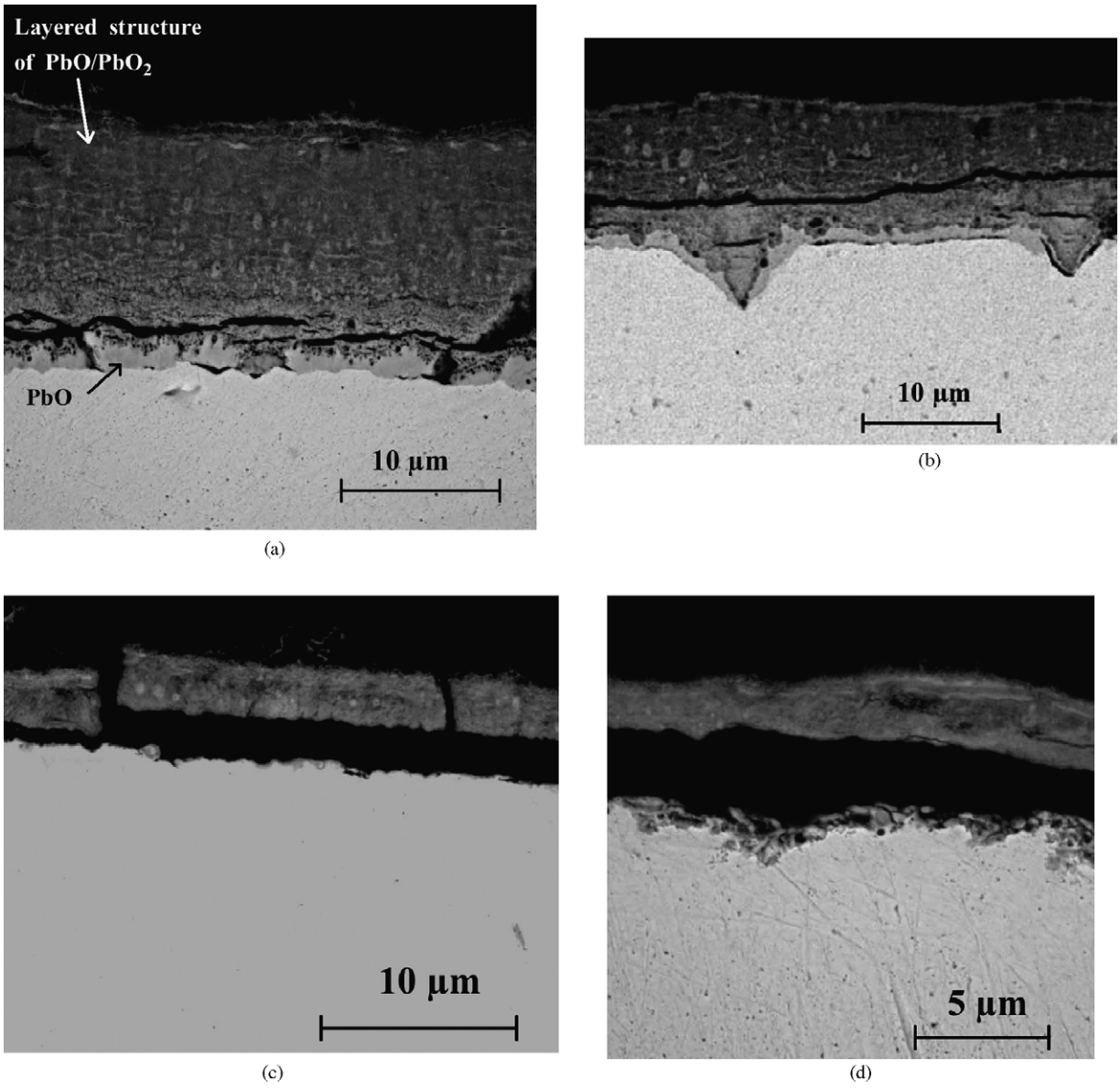

Fig. 12. Metallographic cross-sections of aged PbCaSn alloys after the cycling test: (a) 0 wt.%; (b) 0.6 wt.%; (c) 1.2 wt.%; (d) 2 wt.%.

4.1. Effect of metallurgical state

Lead metal has a low melting point ($T_f = 600$ K), which means that the diffusion of alloying elements can occur at room temperature and provokes many changes in the properties of alloys with time. The change in the mechanical properties of PbCaSn alloys due to the ageing were studied and characterized by many authors [17,11]. Figs. 4 and 6 demonstrate also that the ageing of PbCaSn alloys can have a strong influence on the corrosion rate in overcharge conditions. The weight loss and the oxygen evolution of the overaged alloys are almost systematically higher than that of aged alloys. As shown by a previous study [13], the overageing process cause an increase of tin content in precipitates and a decrease of tin content in the lead matrix, so the bad corrosion resistance of the overaged alloys is closely related to a low tin content in lead matrix all along the overageing process. Another factor responsible for the high corrosion rate in overcharge conditions is the O_2 gas evolution. In lead alloys, the addition of calcium drastically decreases the overpotential of the O_2 evolution on lead; nevertheless, the addition of tin increases it [18,19]. So, the reducing of the tin content in the lead matrix in the overageing process involves a decrease of the O_2 evolution overpotential and an increase of the mechanical action of the O_2 evolution on the corrosion layer.

Thus, the overageing process has a double negative action on the corrosion behavior of PbCaSn alloys in overcharge: decrease of the tin content in matrix weakens its corrosion resistance and increase of the O_2 evolution induces a higher peeling of the corrosion layer.

In deep discharge conditions, the aged alloys have a lower PbO thickness than that measured on overaged alloys. Previous study has proved that the tin content determines the PbO growth rate. A low content (<1%) accelerates the lead by enhancing the ionic transport through a doping in the oxide lattice (Pb^{II}/Sn^{IV})

[14]. Whereas at higher content in the metal (>1.5–2 wt.%), tin oxide precipitates in PbO layer, limits the oxygen diffusion and inhibits the PbO growth. So in PbCaSn alloys, our results show that when a large part of tin is trapped in the intermetallic phases in the overaged state, its doping effect on the PbO growth lowers. In the high tin PbCaSn alloys (>1.5 wt.%), the tin level in the lead matrix is sufficient to completely inhibit the PbO growth whatever the metallurgical state.

4.2. Tin effect

In practice, many authors report that addition of tin has a beneficial effect on the corrosion behavior of the grids in batteries. Our results show that tin allows reducing the metal consummation in overcharge conditions by a decrease of the O_2 evolution, and inhibits the PbO growth responsible of the battery internal resistance increase in discharge conditions.

Nevertheless the tin effect is not only determined by its concentration in the alloys. We have to consider also its availability in the alloys. Indeed, when tin is trapped in large $(Pb_{1-x}Sn_x)_3Ca$ precipitates during the overageing process, tin is generally less efficient. So the limit of tin level for a positive effect on the corrosion behavior effect depends on the calcium level in alloy and the rate of the overageing reaction. Consequently, the effect of a given tin content is closely related to the metallurgical state of alloys.

Even in cycling conditions, the corrosion layer thickness is related to the tin content. Higher the tin content, lower the lead alloy corrosion, as we can see on Fig. 12. Unfortunately, the interface metal/corrosion layer formed on high tin content alloy is very brittle so the corrosion layer may easily peel off. This lab-observation can be correlated by the remarks of some authors who sometimes observe a loss of cohesion between high tin content grid and positive active mass in the positive plates [10]. This loss of cohesion should be due to loss of adherence of the corrosion layer in some cases on high tin level alloys, because of the absence of the PbO layer acting as a self adhesive compound between lead metal and PbO_2.

4.3. Effect of anodic potential

Through this study, we can distinguish four potential zones for the positive grid, with four corrosion behaviors. The first is located at low potentials below +0.7 to +0.8 V and is the typical zone of deep discharge. At these potentials, the corrosion rate is low, but the growth of the insulating corrosion layer quickly increases the battery internal resistance. Previous studies have proved that the PbO growth kinetic is almost linear with time [14,20].

The second potential zone around +0.9, +1 V leads to the formation of complex and thick corrosion layer $Pb/PbO/PbO_x/PbO_2$ where the PbO_x sub-layer seems to be a melt of PbO and PbO_2. In this potential zone, the corrosion is more important than that in the first one and the risk of increase of internal resistance is also important.

The third potential range is limited around +1.3, +1.4 V and is representative of charge state or floating conditions of batteries. The measured oxidation current is very low and the corrosion rate is also very low, which was reported by some authors [15]. In this potential range, only the formation PbO_2 layer takes place without the water oxidation into O_2. The PbO_2 growth is particularly slow and characterized by a logarithmic kinetic law, which was shown by previous *in situ* ellipsometric study [21].

The fourth potential zone corresponds to the overcharge conditions behind +1.5 V, and is characterized by an important intergranular corrosion and oxygen release. The oxidation of water to oxygen has a predominant mechanical effect and tends to break and remove the PbO_2 layer. The high corrosion rate in this potential zone can be explained by a cycle growth/breaking/peeling/growth of the corrosion layer. This

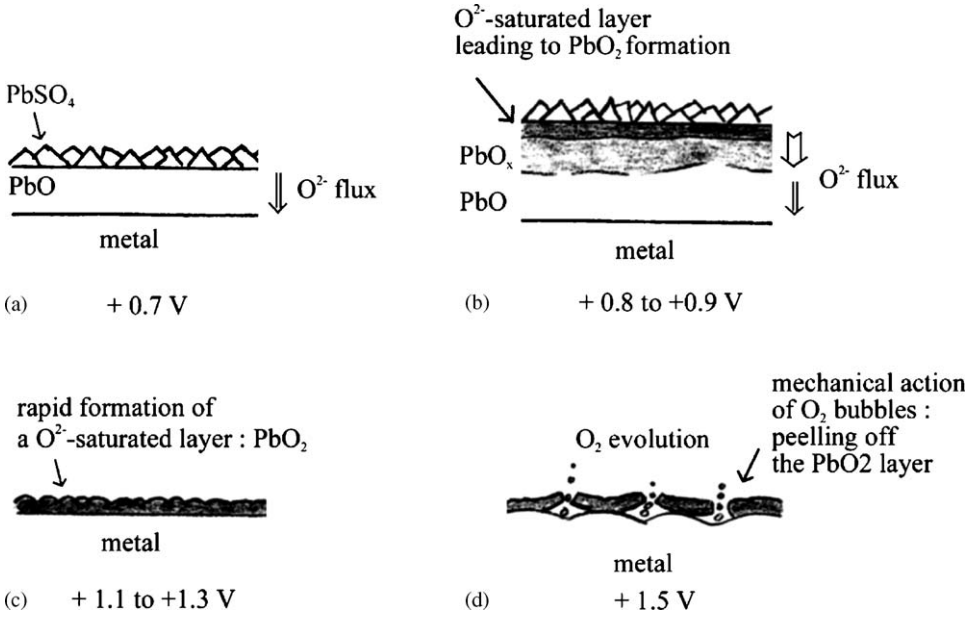

Fig. 13. Schematic mechanism corrosion layer growth on lead alloys in function of potential.

mechanism provokes a rapid consummation of the metal until the mechanical breaking of the grid bars in some cases.

In all the potential range, the mechanism of lead oxidation seems to be governed by the oxygen (O^{2-}) diffusion in the oxide, as displayed on Fig. 13. At low potential (+0.7, +0.8 V), the PbO growth is controlled by the O^{2-} diffusion in the lamellar crystallographic structure of α-PbO, as shown by ^{18}O-tracer experiments [20]. At higher potential (+0.9, +1 V), the O^{2-} diffusion increases until the saturation of the lead monoxide at the interface PbO/electrolyte and leads to the formation of PbO_2/PbO_x. At +1.3 V, the O^{2-} concentration is so high that β-PbO_2 is directly formed on the surface and blocks the O^{2-} diffusion because of its compact rutile crystallographic structure [22]. Then at very high potential, the mechanical effect of the oxygen release is the main responsible of the peeling of the PbO_2 layer and explains the continuous consummation of the metal by a continuous formation of PbO_2.

5. Conclusions

The corrosion management of the positive grids in PbCaSn alloys should take two main factors into account: the composition of the alloy and the electric cycles undergone by the lead batteries. For many applications, a tin level of 1.2–1.6 wt.% seems to be a good compromise. This tin concentration allows the regulation of the O^{2-} diffusion in the corrosion layer especially by limiting the PbO growth, and reduces the O_2 release. Thus, it reduces the mechanical effect of O_2 bubbles which is the main cause of the continuous PbO_2 growth in overcharge conditions. Nevertheless to maintain the beneficial effect of tin in service during the battery lifetime, the tin level in alloys should be adapted to the calcium level and the rate of the overageing process. In fact the efficiency of tin addition is closely related to the metallurgical state of the alloys. According to our results, a Sn/Ca ratio of 2.5 gives the best corrosion resistance in many cases. Nevertheless, when tin level is too high, the corrosion layers can peel off the metal, which involves a lack of cohesion between the collector and the paste in cycling conditions.

The anodic potential is a second main factor determining the alloy corrosion. In service, a too high floating current can maintain the positive alloy grid at a high potential and induces an irreversible corrosion of the positive grids. The same phenomenon occurs when the "boost charges" are too frequent and not closely controlled. In discharge conditions, the cycling at low state-of-charge, for the photovoltaic applications, provokes the formation of a PbO/PbO_x layer by maintaining a low anodic potential of the positive grids. Thus the adjustment of the parameters of the charge controller of a batteries system is a necessity for increasing the lifetime of the grids and for maintaining a good rechargeability.

The challenge for the development of corrosion-resistant grid alloys is a low corrosion rate and an adherent corrosion layer in all the batteries conditions. If additions of tin are nowadays essential, addition of other elements seems to be necessary to improve the adhesion of the oxide of low corrosion rates alloys. These four lab-tests developed in this article may be good tools to test future alloys compositions.

Acknowledgement

This study was financially supported by french governemental organization ADEME (Convention N°9905057).

References

[1] A.F. Hollenkamp, J. Power Sources 36 (1991) 567.
[2] R.D. Prengaman, JOM (2001) 36.
[3] A. Cooper, P.T. Moseley, J. Power Sources 113 (2003) 200.
[4] P. Ruetschi, J. Power Sources 127 (2004) 33.
[5] R.D. Prengaman, J. Power Sources 67 (1997) 267.
[6] N.Y. Tang, E.M.L. Valeriote, J. Sklarchuk, J. Power Sources 59 (1996) 63.
[7] R.J. Ball, R. Kurian, R. Evans, R. Stevens, J. Power Sources 109 (2002) 189.
[8] K.R. Bullock, M.A. Butler, J. Electrochem. Soc. 133 (1986) 1085.
[9] R. Miraglio, R. Albert, A. El Ghachcam, J. Steinmetz, J.P. Hilger, J. Power Sources 53 (1995) 53.
[10] R.D. Prengaman, J. Power Sources 95 (2001) 224.
[11] L. Bouirden, J.P. Hilger, J. Hertz, J. Power Sources 33 (1991) 27.
[12] J.P. Hilger, L. Bouirden, J. Power Sources J. Alloys Compd. 236 (1996) 224.
[13] A. Maitre, G. Bourguignon, J.M. Fiorani, J. Steinmetz, J. Ghanbaja, P. Lailler, Mater. Sci. Eng. A A340 (2002) 103.
[14] E. Rocca, J. Steinmetz, Electrochim. Acta 44 (1999) 4611.
[15] P. Ruetschi, R.T. Angstadt, J. Electrochem. Soc. 111 (1964) 1323.
[16] Y. Yamamoto, K. Fumino, T. Ueda, M. Namlbu, Electrochim. Acta 37 (1992) 199.
[17] H. Borchers, H. Assmann, Metallurgia (Isernberg, Germany) 33 (9) (1979) 936.
[18] B. Monahov, D. Pavlov, D. Petrov, Proceedings of the 14th Annual Battery Conference on Applications and Advances, Long Bead, CA, USA, 1999, pp. 275–279.
[19] L.T. Lam, J.D. Douglas, R. Pillig, D.A.J. Rand, J. Power Sources 48 (1994) 219.
[20] E. Rocca, J. Steinmetz, S. Weber, J. Electrochem. Soc. 146 (1999) 54.
[21] N. Stein, G. Bourguignon, L. Raboin, L. Broch, L. Johann, E. Rocca, Thin Solid Films 455/456 (2004) 735–741.
[22] J. Leciejewiec, I. Padlo, Naturwissenschaften 49 (1962) 373.